Investigating the mixture of a benzotriazole and potassium iodide as efficient inhibitor against acid corrosion of 70Cu–30Ni alloy

[1]ONYEACHU, B. Ikenna, [2]ETIOWO, M. Kokolo, [2]IKPI, E. Magdalene, [2]IKEUBA, Alexander, & [3]OFOR, U. Edith.

[1]College of Science and Computing, Wigwe University Isiokpo, Rivers State, Nigeria.
[2]Department of Chemistry, Cross Rivers State University of Technology, Calabar, Nigeria.
[3]Basic Science Unit, School of Science and Technology, Pan Atlantic University, Lagos, Nigeria.
✉: Ikenna.onyeachu@wigweuniversity.edu.ng; +(234) 8034917997

Received: 28:05:2025 **Accepted: 25:07:2025** **Published: 25:07:2025**

Abstract:
Industrial heat exchangers and cooling systems usually develop scales on their internal walls, which impede fluid flow, diminish their thermal conductivities and, hence, their efficiencies. Restoring these qualities requires pickling with acid solutions, especially, HCl which forms very soluble products of scales. Without adding efficient corrosion inhibitor chemicals to the pickling solutions, serious corrosion attack on the substrates accompanies the acid pickling process. Identifying prospective corrosion inhibitor chemicals with green environmental profile and high efficiencies becomes imperative for many industries. Herein, we employed weight loss, electrochemical impedance spectroscopy (EIS) and potentiodynamic polarization (PDP) to investigate the mixture of 5–methyl–1H–benzotriazole (5MB) and potassium iodide (KI) as efficient corrosion inhibitor systems for heat exchanger-type alloy (70Cu-30Ni) against corrosion in 1 M HCl solution. The addition of KI boosts the inhibition efficiency of 5MB from ≈74 % to ≈96 %. The 5MB + KI mixture impacts a strong anodic shift in corrosion potential (E_{corr}) and boosts the passivation of the alloy. The inhibitor mixture is also very efficient to diminish the extent of surface microstructural degradation of the alloy, based on characterizations by atomic force microscopy (AFM) and scanning electron microscopy (SEM).

Keywords: Copper-nickel alloy; Passivation; Corrosion inhibition; Acid pickling; Polarization.

1. INTRODUCTION

There is a physical and surface microstructural deterioration that occurs when industrial heat exchanger tubes and cooling water systems are subjected to acid corrosion during pickling [1-3]. It is initiated and sustained by the alterations in electrode potential of the alloy due to simultaneous oxidation and reduction reactions occurring on its surface. Although these alloys are selected because of their generally good corrosion resistance, their protective passive layers can succumb to acid attack during industrial pickling activities. Acid pickling is an inevitable industrial practice whereby dilute mineral acids are used to dislodge corrosion and production scales that have developed on the surfaces of heat exchangers and cooling systems [4,5]. Given that chloride ions usually form more dissoluble products with these scales, HCl is the mostly used acid pickling agent in the industry [6,7]. While dissolving the scales, however, the acid also corrodes the underlying alloy substrate, deteriorates its surface microstructure and weakens its material strength. It is for this reason that industries add corrosion inhibitors into the acid solution to block such attack [8-16]. One of the most important alloys for fabricating heat exchangers and cooling water systems is copper-nickel (Cu-Ni) alloys, especially the nickel-rich 70Cu-30Ni.

Cheapness, natural abundance, and environmental benignity are important criteria that edge organic corrosion inhibitors over their inorganic counterparts. They are usually characterized by the presence of nitrogen, oxygen and/or sulfur heteroatoms (held within aromatic rings containing C=C groups). These inhibitors possess free non-bonding and *pi* electrons that interact with d-orbitals of the alloy metal atoms to initiate adsorption and formation of protective hydrophobic surface films [17-20]. For acid corrosion of copper Cu-Ni alloys, azole derivatives (such as benzotriazoles) are sufficiently efficient corrosion inhibitors [21-30]. Deductions from experiments show that the azoles impede the corrosion of copper alloys either through a chemical interaction (leading to a complex formation) or a physical interaction (leading to adsorbed film formation). Furthermore, the efficiencies of acid corrosion inhibitors are significantly boosted by adding very low doses of metal iodides (especially potassium iodide, KI) [31-35]. Since azoles are usually protonated in acid solutions, their adsorption and inhibition efficiencies are significantly boosted in the presence of halide ions, especially iodide ions (I^-). The iodide anions cause the alloy surface to become negatively charged thereby enhancing attraction/interaction between the protonated inhibitor species and the alloy surface.
In this work, we investigate the efficiency of 5–methyl–1H–benzotriazole (5MB), Figure 1, (singly and mixed with KI) to mitigate 70Cu-30Ni corrosion in 1 M HCl solution. Previously, we had reported the efficacy of 5MB and 5MB + KI inhibitor system to protect steel in similar acid system [36].

Our motivation to extend investigation of this inhibitor system to Cu–Ni alloy is because an inhibitor system that can protect a variety of industrial alloys will save cost and maximize profit for the industry. As an environmentally safe molecule, 5MB belongs to category 4 in the globally harmonized system of oral toxicity classification, has a partition coefficient of 1.4, and lethal dosage of 1600 mg/kg [37–39]. For this work, we employ weight loss technique to understand how 5MB (alone and mixed with KI) diminishes the corrosion kinetics. We augment the weight loss results with electrochemical assessment to showcase the mechanism of inhibition, using electrochemical impedance spectroscopy (EIS) and potentiodynamic polarization (PDP). We further employ atomic force microscopy (AFM) and scanning electron microscopy (SEM) to peruse the extent of surface protection provided by the 5MB + KI mixture.

2. EXPERIMENTAL SECTION

2.1. Preparation of inhibitors and alloy substrate

A stock 5MB solution was prepared in isopropanol and calculated aliquot volumes withdrawn from the stock were diluted to 100, 250, 500 and 1000 ppm using the acid solution. Acid solution containing KI was prepared by dissolving 0.166, 0.83 and 1.66 g of KI in the HCl solution. The elemental composition of the 70Cu–30Ni alloy was previously reported [12,26]. The dimensions of specimen used for weight loss gave a working surface area of 23.63 cm^2, whereas the electrochemical specimen was mounted in epoxy resin and the surface area of 1 cm^2 was exposed for the measurements. Before the weight loss or electrochemical testing, the alloy coupons were polished with different grit emery papers (up to 800 grit size), followed ultrasonic cleaning in a mixture of ethanol-water solution, and dried [40].

2.2. Weight loss measurements

Weight loss experiments were performed by immersing duplicate samples of 70Cu–30Ni coupons for 48 h in 200 mL of 1 M HCl without and with (i) 100, 250, 500 and 1000 ppm 5MB, (ii) 1, 5, 10 mM KI, and (iii) 1000 ppm 5MB + 10 mM KI. Post immersion treatment involved retrieving the coupons from test solutions, cleaning them according to the ASTM G1-03 standard procedure [41], and reweighing them to determine weight loss (ΔW) according to Equation (1). From the weight loss, the corrosion rate (υ, mm/yr) was calculated according to Equation (2); such that ρ = density of the 70Cu–30Ni (8.94 g cm^{-3}), T = immersion time (48 h), and A = surface area of the coupons (22.63 cm^2). Similarly, the corrosion inhibition efficiency (% $IE_{\Delta W}$) was calculated from the weight loss results, according to Equation (3).

$$\Delta W\ (\mathrm{g}) = W_{(\text{before immersion})} - W_{(\text{after immersion})} \quad (1)$$

$$\upsilon\ (\mathrm{mm/yr}) = \frac{\Delta W \times 87600}{A \times \rho \times T} \quad (2)$$

$$\%\, IE_{\Delta W} = 1 - \frac{\Delta W_{(\text{with inhibitor})}}{\Delta W_{(\text{without inhibitor})}} \times 100 \quad (3)$$

2.3. Electrochemical assessment

The electrochemical measurements were conducted on a Gamry 600 potentiostat. The experiments were conducted after immersing the alloy for 48 h at 25 °C in the acid solution devoid of and containing the following: (i) 100 to 1000 ppm of 5MB, (ii) 1, 10 mM KI, and (iii) 1000 ppm 5MB + 10 mM KI. The electrochemical circuit consisted of the 70Cu–30Ni coupon as test electrode which had its potential varied with reference to a silver-silver chloride electrode, while a graphite rod completed the circuit as an auxiliary electrode. The criterion for attaining a steady-state equilibrium potential (OCP), prior to any electrochemical corrosion testing, was satisfied by allowing the coupons to corrode freely in the various test solutions for thirty minutes. The parameters for EIS characterization were as follows: (i) sinusoidal potential perturbation = 10 mV vs. OCP, and (ii) frequency range = 10^5 Hz to 10^{-2} Hz. The parameters for the PDP characterization were as follows: (i) potential scan range = (–0.25 V vs. OCP) to (+1.70 V vs. Ref.), and (ii) potential scan rate = 0.5 mV/s. The efficiency of corrosion inhibition (*% IE*) was estimated from the respective electrochemical techniques based on Equations (4 & 5).

$$\%\, IE_{\mathrm{EIS.}} = 1 - \frac{R_{\mathrm{total(without\ inhibitor)}}}{R_{\mathrm{total(with\ inhibitor)}}} \times 100 \quad (4)$$

$$\%\, IE_{\mathrm{PDP}} = 1 - \frac{i_{\mathrm{corr(with\ inhibitor)}}}{i_{\mathrm{corr(without\ inhibitor)}}} \times 100 \quad (5)$$

2.4. Surface characterization

After allowing the alloy to corrode freely in the acid solution for 48 h without and with 5MB + KI, the surface morphology was observed with the aid of an atomic force microscope (Stromilingo DIY AFM), Thereafter, the Gwydion software embedded in the AFM instrument was further employed to analyze the images and obtain three-dimensional images of the bare and pre-corroded alloys in addition in the statistical analysis of the generated images. Additionally, we ascertained the extent of surface degradation using the Ziess Evo 50 XVP scanning electron microscope.

3. FINDINGS AND DISCUSSION

3.1. Weight loss

The extent by which 5MB mitigates against the corrosion of 70Cu–30Ni alloy is evidenced by the weight loss and corrosion rate values in Table 1. The addition of 5MB consistently suppressed the weight loss experienced by the alloy from 0.032 g ± 0.007 (in the absence of inhibitor) to 0.008 g ± 0.001 (with 1000 ppm 5MB). This amounted to a corrosion inhibition efficiency approximately 75 % delivered by the maximum inhibitor dose tested. By lowering the amount of weight loss experienced by the alloy, 5MB exhibits the ability to block reactive anode and cathode sites where rapid oxidation and reduction reactions are occurring concurrently on the alloy surface. The loss in weight during corrosion usually occurs predominantly due to anodic processes like Cu and Ni oxidation into Cu^+/Cu^{2+} and Ni^{2+}, respectively [42,43]. The electrons released from these anodic sites are simultaneously taken up at cathodic sites to sustain the reduction reaction.

Given that copper (Cu), the parent metal in the alloy, is more noble than hydrogen (H) in the electrochemical series, it is unlikely that

$$2H^+ + 2e^- = H_2$$

would be the major cathodic reaction. Rather, the Cu and Ni dissolution at anodic sites would be sustained by the cathodic reduction of oxygen

$$4H^+ + O_2 + 4e^- = 2H_2O$$

as previously reported [44]. This blockage of active sites is courtesy of adsorbed 5MB molecules. The adsorption can mitigate either (or both) anodic and cathodic reactions. Anodic reactions are blocked via the donation of lone electron pairs from the triazole nitrogen atoms into the incompletely–filled d–orbitals of Cu and Ni atoms. The donation of electrons into these orbitals suppresses the propensity for the atoms to oxidize. In addition, 5MB can also adsorb on anodic sites via the electrostatic attraction between its protonated form and anionic species (like Cl^-) already pre-adsorbed (due to enormous Cu^+/Cu^{2+} and Ni^{2+} cations generated at such sites). On the other hand, 5MB adsorption can truncate cathodic reactions because its protonated molecules competitively adsorb to lower the influence of H^+ on the reduction of O_2. Since the 5MB is larger in size than H^+, its adsorption would cover more cathodic surface area, increase the hydrophobicity of the cathodic regions, and shunt the electrochemistry of the corrosion process. This explains why 5MB addition reduces the extent of weight loss experienced by 70Cu–30Ni alloy during corrosion in 1 M HCl solution.

Thermodynamically, the mode of adsorption demonstrated by organic corrosion inhibitors on metal surfaces can be described by fitting corrosion inhibition efficiency/surface coverage and inhibitor concentration data into adsorption isotherms. In this work, 5MB adsorption on the Cu-Ni surface was tested by fitting results into the Langmuir, Temkin and Freundlich isotherms. According to the Equation (6), a direct proportionality between the degree of surface coverage by inhibitor (θ) and the inhibitor concentration (C) indicates a Langmuir-type adsorption (where only a monolayer of adsorbed inhibitor forms on the surface, and that inhibitor-inhibitor interactions are insignificant) [45]. A Temkin-type adsorption follows Equation (7) and yields a straight line in the plot of θ vs. ln *C*. If inhibitor adsorbs via the Temkin model, as depicted by Equation (8), it implies that inhibitor molecules partake in some positive or negative interaction with one another, which usually leads to the formation of homogenous or heterogenous multilayer on the alloy surface. The degree of inhibitor interaction is deduced from the value of (α) [46]. On the other hand, a Freundlich-type adsorption requires a direct proportionality between the logarithms of θ and C, from which the degree of metal surface heterogeneousness and intensity of inhibitor adsorption ($\frac{1}{n}$) can be extrapolated. The Freundlich-type adsorption is very probable if $0 < \frac{1}{n} < 1$, but is modest or improbable, respectively, if $\frac{1}{n} = 1$ or $\frac{1}{n} > 1$ [47]. As Figure 2(a) reveals, the Langmuir isotherm describes, most accurately, the mode of 5MB adsorption on the Cu-Ni alloy surface because the plot exhibits the best agreement between experimental and fitting plots and has the highest R^2 value, compared with the Temkin and Freundlich models in Figures 2(b) and (c), respectively. Furthermore, the thermodynamic spontaneity with which 5MB adsorbs to form the monolayer film was predicted from the ΔG_{ads} value, according to the relationship in Equation (9) whereby R is the universal gas constant (8.314 J $K^{-1}mol^{-1}$), T is absolute temperature, and the amount of water molecules is 10^6 ppm [48]. The calculated negative value of $\Delta G_{ads} = -23.89\ kJ\ mol^{-1}$ is consistent with a spontaneous and highly feasible inhibitor adsorption.

$$\frac{C}{\theta} = \frac{1}{K_{ads}} + C \quad (6)$$

$$\theta = -\frac{1}{2\alpha}\ln C - \frac{1}{2\alpha}K_{ads} \quad (7)$$

$$\log\theta = \log K_{ads} + \frac{1}{n}\log C) \quad (8)$$

$$\Delta G_{ads} = -RT\ln(10^6 K_{ads}) \quad (9)$$

The addition of KI also impacted positively on the corrosion resistance of the alloy. According to Table 1, the maximum KI concentration (10 mM) delivers an inhibition efficiency of approximately 59 %. The application of KI to boost the efficiency of conventional acid–cleaning corrosion inhibitors is well–known. The I^- ions from KI interact with the abundant Cu^+/Cu^{2+} and Ni^{2+} ions to form thin films of insoluble iodides. Although the corrosion–causing Cl^- ions are the more abundant anions in the acid solution (and are also capable of similar interaction with Cu^+/Cu^{2+} and Ni^{2+} ions), the larger ionic radius of I^- ion enables it to displace a Cl^- ion from the alloy surface and lower the corrosion rate [49]. According to Table 1, the mixture of 1000 ppm 5MB + 10 mM KI impacts a marked increase in corrosion inhibition efficiency to approximately 94 %. It showcases an important synergism between 5MB and I^- ions. It is rational to attribute the enhanced adsorption of 5MB to the effect of I^- ions which induce a net negative charge on the corroding metal surface and, therefore, attract more cationic species in the solution, especially the protonated 5 MB molecules. This synergism could either be competitive or cooperative depending on the calculated value of synergism parameter (S_θ) based on Equations (10 & 11), whereby $\theta_{1+2} = \theta_1 + \theta_2 - (\theta_1\theta_2)$, θ_1 = degree of surface coverage by 5MB, θ_2 = degree of surface coverage by I^- ions, and θ'_{1+2} = the degree of surface coverage by 5MB + I^- ions. A competitive synergism, $S_\theta < 1$, suggests that both 5MB molecules and I^- ions compete for adsorption sites, whereas cooperative synergism ($S_\theta \geq 1$) indicates that the adsorption of I^- ions create a template on the alloy surface that improves the adsorption of 5MB. From the values in Table 1, the calculated value of $S_\theta = 1.6248$ strongly indicates a cooperative synergism offered by I^- ions towards 5MB adsorption. Similar mechanism of interaction between 5MB and I^- ions was also reported during the inhibition of carbon steel corrosion in 1 M HCl [45].

$$S_\theta = \frac{1-\theta_{1+2}}{1-\theta'_{1+2}} \quad (10)$$

$$\theta = \frac{\%\ \mathrm{IE}}{100} \quad (11)$$

3.2. Electrochemical characterization results

3.2.1. Electrochemical Impedance Spectroscopy (EIS)

The impedance behavior of 70Cu-30Ni alloy after 48 h immersion in the blank and inhibited acid solutions is expressed as the Nyquist plots in Figure 3(a). Under the investigated conditions, the alloy exhibited two Nyquist arcs comprising a small arc at the high frequency and a wider arc spanning into the low frequency region. Similar characteristics were reported in previous works [12,26,50]. The two Nyquist arcs portray two phenomena taking place on the alloy surface. The first arc at high frequency is the phenomenon that signals a corrosion layer-solution interface, whereas the second arc at low frequency signals the phenomenon beneath the corrosion layer (i.e. the corrosion layer-substrate interface). Two-time constants, as displayed in the Nyquist plots, are commonly modelled with the electrical equivalent circuit model in Figure 3(b). The values of electrical elements R_f and CPE_f describe the corrosion layer-solution interface. The element R_f showcases the resistance of corrosion layer to porosity, while the CPE_f is a constant phase element defined by an admittance, Y_f, and a roughness parameter, α_f [50]. Higher values of R_f and lower values of Y_f are indices of a protective corrosion layer-solution interface. On the other hand, the low frequency arc provides information about the dielectrics of charges that have penetrated beneath the corrosion layer (qualitatively assessed from the value of double layer admittance, Y_{dl}) and the kinetics of charge transfer (deduced from the charge transfer resistance, R_{ct}). Whereas Y_{dl} and Y_f portray the extent of charge accumulation permitted by the corrosion layer, the combination of R_f and R_{ct} accounts for the effective resistance to corrosion (R_p) experienced by the Cu-Ni alloy.

The arc sizes are obviously larger when corrosion inhibitors are present in the solution, following the increasing order of magnitude: KI < 5MB < 5MB + KI. Larger arcs are indicators of higher corrosion resistance. Using the Echem Analyst software embedded within the potentiostat, we extrapolated values for all the electrical elements that define the impedance characteristics of the alloy in the absence and presence of corrosion inhibitor systems. The values are detailed in Table 2. The R_s is the solution resistance, which is a measure of isolation between the corroding surface and the solution [51]. Higher values of R_s are attributed to increased isolation of corroding surface away from the corrosion agents (i.e. greater corrosion resistance). The elements α_f and α_{dl} ($-1 \leq \alpha \leq 1$) indicate the extent of corrosion-induced surface roughness/inhomogeneity of the different interfaces, as well as the inclination of the interface to behave like a resistor, capacitor or inductor [50]. Both elements Y and α are components of the constant phase element (CPE) which is a more reliable parameter for describing interfacial phenomena like adsorption of species (e.g. aqueous ions and corrosion inhibitors) on a solid (corroding electrode) surface. The impedance of a CPE (Z_{CPE}) is described by Equation (12); where j is an imaginary unit ($j = -1)^{1/2}$, w represents the angular frequency.

$$Z_{CPE} = Y_0^{-1}(jw)^{-\alpha} \quad (12)$$

From Table 2, R_s has persistently higher value when a corrosion inhibitor is present, changing from 0.90 Ω cm^2 in the blank solution to 1.91, 1.20 and 2.49 Ω cm^2, respectively, in the presence of 5MB, KI and 5MB + KI. These values reveal the extent to which the different inhibitors isolate the alloy surface from corrosion agents. Although the alloy shows tendency to form a corrosion layer (given that it also displays two Nyquist arcs in the absence of inhibitors), the corrosion inhibitors (especially the 5MB + KI mixture) significantly improve the protection ability of the corrosion layer. The inhibitors do this by adsorbing on the alloy surface to displace water molecules and form hydrophobic organic layers that isolate the alloy surface from the acid solution. Furthermore, the highest inhibition efficiency delivered by 5MB + KI system confirms that the iodide ions effectively promote the adsorption of protonated organic molecules, as described in the previous section. Consequently, the resistance parameters (R_f and R_{ct}) are higher while the admittance parameters (Y_f and Y_{dl}) are lower in the presence of corrosion inhibitors. The inhibitor 5MB delivers a maximum efficiency approximately 74 %, which significantly increases to 96 % when 10 mM KI is added. Furthermore, the presence of corrosion inhibitors also increases the values of α, with the highest values registered in the presence of 5MB + KI. This suggests that the adsorption of corrosion inhibitors also lowers the roughness attributes of the formed corrosion layer, thus, making it smoother, more adherent to substrate and less porous.

3.2.2. Potentiodynamic Polarization

Results obtained after potentiodynamic polarization of 70Cu-30Ni alloy in HCl solution is depicted in Figure 3(c). Normally, corrosion in the acid solution constitutes an electrochemical process whereby electrons shuttle between anode and cathode active sites on the alloy surface due to simultaneous oxidation and reduction reactions. Therefore, potentiodynamic polarization (PDP) techniques can elucidate the rate at which these processes occur (i.e. corrosion rate) and the mechanism by which a corrosion inhibitor system can impede the processes. The addition of 5MB to the acid solution minimally affects the cathodic reactions but markedly affects the anodic reactions. Given that Cu and Ni are more noble than hydrogen in the electrochemical series, direct H^+ reduction into H_2 gas would not be a thermodynamically feasible cathodic reaction in the acid. Rather, the most feasible cathodic process would be the reduction of oxygen in the presence of H^+ ions, as shown in Equation (13) [52]. The cathodic reactions are sustained by continuous electron supply from anodic sites where Cu/Ni oxidation predominantly occur, based on Equations (14) and (15). The polarization curves are similar in shapes both in the blank and inhibited acid solutions, showcasing a significant improvement of anodic and passivation processes unlike the cathodic reactions.

$$O_2 + 4H^+ + 4e^- = 2H_2O \quad (13)$$

$$Cu = e^- + (Cu^+) = e^- + Cu^{2+}) \quad (14)$$

$$Ni = 2e^- + Ni^{2+} \quad (15)$$

When the cathodic–anodic arms of the PDP curves are extrapolated around ± 10 mV of their transition points, the corrosion potential (E_{corr}), corrosion current density (i_{corr}), anodic (β_a) and cathodic (β_c) Tafel constants, as well as passivation potentials (E_{pass}) and current density (i_{pass}) were extrapolated [32], and the values are presented in Table 3. The i_{corr}, an indicator of corrosion rate, obviously decreases as the 5MB concentration increases. A maximum inhibition efficiency approximately 73 % is recorded when 1000 ppm was added. The KI addition similarly lowered i_{corr} with 10 mM concentration delivering 55 % efficiency. These results agree well with the determinations from weight loss and EIS characterizations. Furthermore, the values of cathodic Tafel (β_c) do not change appreciably with respect to the blank, unlike the observation for anodic Tafel (β_a). Passivation potential and current are also lower in the presence of inhibitor (especially with 5MB + KI mixture), which implies greater inclination to form protective corrosion layer due to the presence of inhibitor systems. Furthermore, the passivation current (i_{pass}) describes the extent of protectiveness provided by the different corrosion layers formed by the alloy. The lower the value of i_{pass}, the less porous and more protective is the corrosion layer.

The anodic portion of the PDP curve shows an active region followed by a stable passivation. The observed passivation endorses the two Nyquist arcs observed in the EIS results. It strongly proves that 5MB, KI and their mixture are more inclined to blocking active sites where Cu and Ni are lost via oxidation. The inhibitor systems promote the conversion of Cu and Ni atoms into more protective corrosion products. The mechanisms by which these active sites can be blocked by 5MB and its mixture with KI has been highlighted in the previous sections. From the PDP curve, we observe that the organic inhibitor alone induces wider passivation potential range and lower passivation current, compared with the inorganic KI. It implies that an organic surface film formed by 5MB is more protective than the inorganic products formed by iodide ions. Therefore, a hydrophobic surface film is more formidable to protect the Cu-Ni alloy during corrosion in the HCl solution. When 5MB is combined with KI, we observe a clear anodic shift of corrosion potential (E_{corr}) and a new passivation phenomenon. Upon closer comparison, we notice an attempt for this new passivation to occur for the uninhibited alloy, although it does not last. When 5MB and KI are combined, this new passivation is now more stable but somewhat short-lived. The resistance exhibited by Cu-Ni alloys during corrosion in acid solutions is usually attributed to the formation of Cu_2O passive layer [53,54]. However, the Cu_2O formation is preceded by the combination of Cu^+ and Cl^- ions to precipitate insoluble CuCl which triggers a primary, short-lived passivation [53–55]. It can be reasoned that the CuCl primary passivation is more emboldened and stabilized when the alloy surface is more protected from corrosion attack.

3.3. Surface characterization

After immersing 72 h in the acid solution without and with 5MB + KI, surface morphology of the alloy was probed using atomic force microscopy (AFM) and the acquired data were analyzed with Gwydion software. The images are depicted in Figures 4 (a) and (b) for the blank and inhibited conditions, respectively. The average surface roughness in the blank solution was 0.2045 nm, while it was 0.1330 nm due to the addition of inhibitor. The lower roughness value due to inhibitor addition confirms a diminished extent of corrosion-induced surface degradation. In Figures 4(c) and (d), the surface microstructure of the Cu-Ni alloy is presented after corroding in the acid solution without and with 5MB + KI. In Figure 4(c), the alloy surface experiences severe degradation with several cracks and grain boundary destruction. It confirms a highly corroded surface without an inhibitor system. However, the alloy surface suffers less damage in the acid containing 5MB + KI, as Figure 4(d) showcases. This is affirmation of the weight loss and electrochemical results which prove that the corrosion of 70Cu-30Ni alloy in the HCl acid solution can be effectively mitigated by the mixture of 5MB + KI.

4. Conclusion

In this present work, we augmented weight loss and electrochemical techniques with surface probe analytical techniques like AFM and SEM to investigate the efficiency of 5MB, alone and its mixture with KI, to mitigate the corrosion and surface degradation of 70Cu-30Ni in 1 M HCl solution. Based on the results obtained, we can conclude as follows:

1. 70Cu-30Ni alloy can protect itself from corrosion in 1 M HCl solution by forming some corrosion layer after 48 h exposure.
2. 5MB interacts with the Cu-Ni surface by adsorbing to improve the protectiveness of the corrosion product layer formed by the alloy, and this adsorption follows the Langmuir isotherm model.
3. The addition of KI to 5MB confers some anodic influence on its corrosion inhibition mechanism and significantly enhances the inhibition efficiency above 90 %.
4. The 5MB + KI mixture also promotes the stability of primary and secondary passivation of Cu-Ni alloy in the acid solution.
5. The destruction of surface microstructure due to Cu-Ni corrosion is strongly mitigated by the 5MB + KI mixture.

Declaration of conflict of interests

The authors declare no conflict of interest.

Acknowledgements

The authors acknowledge the African Center of Excellence in Future Energies and Electrochemical Systems (ACE-FUELS), Federal University of Technology Owerri, for providing some of the research facilities for this work.

References

[1] M. Ali, A. Ul-Hamid, T. Khan, A. Bake, H. Butt, O.E. Bamidele, and A. Saeed, "Corrosion-related failures in heat exchangers", *Corrosion Reviews,* vol. 39, no. 6, pp. 519-546, 2021. https://doi.org/10.1515/corrrev-2020-0073.

[2] H. Ezuber, and S.M. Zakir Hossain, "A review of corrosion failures in shell and tube heat exchangers: roots and advanced counteractive", *Heat and Mass Transfer* vol. 59, no. 6, pp. 971-87, (2023). https://doi.org/10.1007/s00231-022-03301-3.

[3] O. Opel, M. Wiegand, K. Neumann, M. Zargari, and S. Plesser, "Corrosion in heating and cooling water circuits-A field study", *Energy Procedia,* vol. 155, pp. 359-66, 2018. https://doi.org/10.1016/j.egypro.2018.11.042.

[4] A.A. Meroufel, "Corrosion Control during Acid Cleaning of H 5 Exchangers', In: Saji, V.S., Meroufel, A.A., Sorour, A.A. (eds) *Corrosion and Fouling Control in Desalination Industry* (Springer), pp. 209-224, 2020. https://doi.org/10.1007/978-3-030-34284-5_10.

[5] N. Mohammadaliha, M. Amani, and M. Bahrami, "Thermal performance of heat and water recovery systems: Role of condensing heat exchanger material", Cleaner Engineering and Technology" vol. 1, pp. 100024, 2020. https://doi.org/10.1016/j.clet.2020.100024.

[6] T. Hodgkiess, K.H. Al-Omari, N. Bontems, and B. Lesiak, "Acid cleaning of thermal desalination plant: do we need to use corrosion inhibitors"? *Desalination*, vol. 183, pp 209-216, 2005. https://doi.org/10.1016/j.desal.2005.03.036.

[7] I.B. Obot, I.B. Onyeachu, N. Wazzan, and A.H. Alamri, "Theoretical and experimental investigation of two alkyl carboxylates as corrosion inhibitors for steel in acidic medium", *Journal of Molecular Liquids*, vol. 279, pp. 190-207, 2019. https://doi.org/10.1016/j.molliq.2019.01.116.

[8] A.H. Alamri, K. Rasheeda, S.J. Kamal, M. Aljohani, T.A. Aljohani, I. Baig, V.D. Alva, N.P. Swathi, I.B. Onyeachu, and S. Samshuddin, "Pyrimidine derivatives as efficient anticorrosive agents for acid corrosion of mild steel: Electrochemical and computational validation", *Arabian Journal of Chemistry*, vol. 17, no. 6, pp. 105752, 2024. https://doi.org/10.1016/j.arabjc.2024.105752.

[9] A.C. Njoku, D.I. Njoku, S.C. Nwanonenyi, P.I. Anyanwu, I.B. Onyeachu, and B. El Ibrahimi, "Anticorrosion performance of nicotinic acid and nicotinic acid hydrazide blended with optimized potassium iodide against Q235 steel corrosion in acid-chloride medium", *Journal of Molecular Structure*, vol. 1297, pp. 136861, 2024. https://doi.org/10.1016/j.molstruc.2023.136861.

[10] I.B. Onyeachu, I.B. Obot, and E.E. Oguzie, "Anticorrosion performance of 1–benzylimidazole and synergistic iodide additives on C1018 carbon steel in 15% HCl solution", *Materials Today Communications*, vol. 36, 106407, 2023. https://doi.org/10.1016/j.mtcomm.2023.106407.

[11] J.E. Eziuka, I.B. Onyeachu, D.I. Njoku, S.C. Nwanonenyi, M.A. Chidiebere, and E.E. Oguzie, "Elucidating the inhibition behaviour of *Pterocarpus santalinoides* leaves extract on mild steel corrosion in H_2SO_4 solution–GC-MS, FTIR, SEM, Experimental and computational approach", *Moroccan Journal of Chemistry*, vol. 11, no. 3, pp. 579-593, 2023. https://doi.org/10.48317/IMIST.PRSM/morjchem-v14i03.39198.

[12] I.C. Ukaga, P.C. Okafor, I.B. Onyeachu, A.I. Ikeuba, and D.I. Njoku, "The inhibitive performance of 2, 3-pyrazine dicarboxylic acid and synergistic impact of KI during acid corrosion of 70/30 and 90/10 copper–nickel alloys", *Materials Chemistry and Physics*, vol. 296, pp. 127313, 2023. https://doi.org/10.1016/j.matchemphys.2023.127313.

[13] D.Y. Wang, Z.G. Li, Y. Liu, H.J. Li, and Y.C. Wu, "Investigation of efficient corrosion inhibitor during acid cleaning of reverse osmosis (RO) desalination plant", *Corrosion Science,* vol. 208, pp. 110609, 2022. https://doi.org/10.1016/j.corsci.2022.110609.

[14] M. Motamedi, A.R. Tehrani-Bagha, and M. Mahdavian, "Effect of aging time on corrosion inhibition of cationic surfactant on mild steel in sulfamic acid cleaning solution", *Corrosion science*, vol. 70, pp. 46-54, 2013. https://doi.org/10.1016/j.corsci.2013.01.007.

[15] K. Haruna, O.C. Al Hamouz, and T.A. Saleh, "The corrosion inhibition performance of a diissocyanate-imidazole based organic compound during acid cleaning of MSF desalination plant", *Heliyon*, vol. 10, no. 19, pp. e38116, 2024. https://doi.org/10.1016/j.heliyon.2024.e38116.

[16] A.H. Alamri, and I.B. Obot, "Highly efficient corrosion inhibitor for C1020 carbon steel during acid cleaning in multistage flash (MSF) desalination plant", *Desalination*, vol. 470, pp. 114100, 2019. https://doi.org/10.1016/j.desal.2019.114100.

[17] A. Singh, K.R. Ansari, I.H. Ali, B.E. Ibrahimi, N.R. Sharma, A. Bansal, A.K. Alanazi, M. Younas, A.H. Alamri, and Y. Lin, "Heteroatomic organic compound as a novel corrosion inhibitor for carbon steel in sulfuric acid: Detail experimental, surface, molecular docking and computational studies", *Colloids and Surfaces A: Physicochemical and Engineering Aspects*, vol. 673, pp. 131692, 2023.

[18] L. Guo, I.B. Obot, X. Zheng, X. Shen, Y. Qiang, S. Kaya, and C. Kaya, "Theoretical insight into an empirical rule about organic corrosion inhibitors containing nitrogen, oxygen, and sulfur atoms" *Applied Surface Science*, vol. 406, pp. 301-306, 2017. https://doi.org/10.1016/j.apsusc.2017.02.134.

[19] C. Verma, D.K. Verma, E.E. Ebenso, and M.A. Quraishi, "Sulfur and phosphorus heteroatom-containing compounds as corrosion inhibitors: An overview", *Heteroatom Chemistry*, vol. 29, pp. e21437, 2018. https://doi.org/10.1002/hc.2143.

[20] A.H. Al-Amri, I.B. Onyeachu, J.O. Anyanwu, and E.U. Ofor, "Time evolution and temperature studies of 2-(hydroxymethyl) benzothiazole and its mixture with KI as an inhibitor for steel in 15 % HCl", Journal of Molecular Liquids, vol. 430. Pp. 127762, 2025. https://doi.org/10.1016/j.molliq.2025.127762.

[21] M.A. Domínguez-Crespo, L.G. Zepeda-Vallejo, A.M. Torres-Huerta, S.B. Brachetti-Sibaja, D. Palma-Ramírez, A.E. Rodríguez-Salazar, and D.E. Ontiveros-De La Torre, "New triazole and isoxazole compounds as corrosion inhibitors for Cu-Ni (90/10) alloy and galvanized steel substrates", *Metallurgical and Materials Transactions A*, vol. 51, pp. 1822-1845, 2020. https://doi.org/10.1007/s11661-019-05615-0.

[22] A.A. Khadom, and A.S. Yaro, "Modeling of corrosion inhibition of copper-nickel alloy in hydrochloric acid by benzotriazole", *Russian Journal of Physical Chemistry A*, vol. 85, pp. 2005-2012, 2011. https://doi.org/10.1134/S0036024411110148.

[23] A.A. Khadom, "Dual function of benzotriazole as copper alloy corrosion inhibitor and hydrochloric acid flow improver", *Surface Engineering and Applied Electrochemistry*, vol. 50, pp. 157-172, 2014. https://doi.org/10.3103/S1068375514020069.

[24] A.A. Khadom, and A.S. Yaro, "Mass transfer effect on corrosion inhibition process of copper–nickel alloy in hydrochloric acid by Benzotriazole", *Journal of Saudi Chemical Society*, vol. 18, no. 3, pp. 214-219, 2014. https://doi.org/10.1016/j.jscs.2011.06.013.

[25] A.T. Simonović, Z.Z. Tasić, M.B. Radovanović, M.B. Petrović Mihajlović, and M.M. Antonijević, "Influence of 5-chlorobenzotriazole on inhibition of copper corrosion in acid rain solution", *ACS Omega*, vol. 5, no. 22, pp. 12832-12841, 2020. https://doi.org/10.1021/acsomega.0c00553.

[26] I.B. Onyeachu, M.M. Solomon, S.A. Umoren, I.B. Obot, and A.A. Sorour, "Corrosion inhibition effect of a benzimidazole derivative on heat exchanger tubing materials during acid cleaning of multistage flash desalination plants", *Desalination*, vol. 479, pp. 114283, 2020. https://doi.org/10.1016/j.desal.2019.114283.

[27] L. Alamiparvin, E.G. Kalhor, S.R. Nabavi, S. Ebrahimi, and A. Farzamnia, "Studies on corrosion inhibitor activity of azoles for copper", *Advanced Science Letters*, vol. 23, no. 11, pp. 11293-11297, 2017. https://doi.org/10.1166/asl.2017.10269.

[28] M. Finšgar, "2-Mercaptobenzimidazole as a copper corrosion inhibitor: Part I. Long-term immersion, 3D-profilometry, and electrochemistry", *Corrosion Science*, vol. 72, pp. 82-89, 2013. https://doi.org/10.1016/j.corsci.2013.03.011.

[29] Z. Tasić, M.M. Petrović, M. Radovanović, and M. Antonijević, "5-chloro-1H-benzotriazole and potassium sorbate as binary corrosion inhibitor of copper in acidic solution", *Zastita Materijala*, vol. 59, no. 2, pp. 206-215, 2018. https://doi.org/10.5937/ZasMat1802206T.

[30] M. Mumelaš, H. Otmačić Ćurković, D. Mikić, M. Hranjec, and M. Cindrić, "Benzimidazole derivatives as copper alloy corrosion inhibitors", *Croatica Chemica Acta*, vol. 91, no. 4, pp. 513-523, 2018. https://doi.org/10.5562/cca3450.

[31] I.B. Onyeachu, I.B. Obot, A.H. Alamri, and C.A. Eziukwu, "Effective acid corrosion inhibitors for X60 steel under turbulent flow condition based on benzimidazoles: electrochemical, theoretical, SEM, ATR-IR and XPS investigations", *The European Physical Journal Plus*, vol. 135, no. 1, pp. 129, 2020. https://doi.org/10.1140/epjp/s13360-020-00167-4.

[32] I.B. Onyeachu, M.M. Solomon, K.K. Adama, C.F. Nnadozie, C.C. Ahanotu, C.E. Akanazu, and D.I. Njoku, "Exploration of the potentials of imidazole-based inhibitor package for heat exchanger-type stainless steel during acid cleaning operation", *Arabian Journal of Chemistry*, vol. 15, no. 6, pp. 103837, 2022. https://doi.org/10.1016/j.arabjc.2022.103837.

[33] Y. Wang, Y. Qiang, H. Zhi, B. Ran, and D. Zhang, "Evaluating the synergistic effect of maple leaves extract and iodide ions on corrosion inhibition of Q235 steel in H_2SO_4 solution", *Journal of Industrial and Engineering Chemistry*, vol. 117, pp. 422-433, 2023. https://doi.org/10.1016/j.jiec.2022.10.030.

[34] S. Abd El Wanees, M.M. Kamel, M. Ibrahim, S.M. Rashwan, Y. Atef, and M.G. Abd Elsadek, "Corrosion inhibition and synergistic effect of ionic liquids and iodide ions on the corrosion of C-steel in formation water associated with crude oil", *Journal of Umm Al-Qura University for Applied Sciences*, vol. 10, no. 1, pp. 107-119, 2024. https://doi.org/10.1007/s43994-023-00084-z.

[35] H. Lgaz, A. Chaouiki, M. Chafiq, R. Salghi, H. Tachallait, K. Bougrin, H.Y. Chi, C. Kwon, and I.M. Chung, "Evaluating the corrosion inhibition properties of novel 1, 2, 3-triazolyl nucleosides and their synergistic effect with iodide ions against mild steel corrosion in HCl: A combined experimental and computational exploration", *Journal of Molecular Liquids*, vol. 338, pp. 116522, 2021. https://doi.org/10.1016/j.molliq.2021.116522.

[36] I.B. Onyeachu, and M.M. Solomon, "Benzotriazole derivative as an effective corrosion inhibitor for low carbon steel in 1 M HCl and 1 M HCl + 3.5wt.% NaCl solutions", *Journal of Molecular Liquids*, vol. 313, pp. 113536, 2020. https://doi.org/10.1016/j.molliq.2020.113536.

[37] Protocols on Methods for the Testing of Chemicals Used in the Offshore Oil Industry, Paris Commission (PARCOM), Paris, France, 2006.

[38] United Nations Globally, Harmonized System of Classification and Labeling of Chemicals (GHS), (Retrieved January, 11, 2025 http://www.unece.org/trans/danger/publi/ghs/ghs_rev00/00files_e.html).

[39] 5-Methyl-1H-benzotriazole, U.S. National Library of Medicine, (Retrieved January 20, 2025. (https://pubchem.ncbi.nlm.nih.gov/compound/5-Methyl-1H-benzotriazole).

[40] Y.H. Wang, and J.B. He, "Corrosion inhibition of copper by sodium phytate in NaOH solution: cyclic voltabsorptometry for in situ monitoring of soluble corrosion products", *Electrochimica Acta*, vol. 66, pp. 45–51, 2012. https://doi.org/10.1016/j.electacta.2012.01.063.

[41] ASTM-G 01–03, Standard practice for preparing, cleaning, and evaluation corrosion test specimens, ASTM Book of Standards (Re-approved 1997).

[42] H.H. Strehblow, "Passivity of metals studied by surface analytical methods, a review", *Electrochimica Acta*, vol. 212, pp. 630-648, 2016. https://doi.org/10.1016/j.electacta.2016.06.170.

[43] V. Maurice, and P. Marcus, "Progress in corrosion science at atomic and nanometric scales", *Progress in Materials Science*, vol. 95, pp. 132-171, 2018. https://doi.org/10.1016/j.pmatsci.2018.03.001.

[44] A.M. Shams El Din, M.E. El Dahshan, and A.M. Taj El Din, "Dissolution of copper and copper-nickel alloys in aerated dilute HCl solutions", *Desalination*, vol. 130, pp. 89-97, 2000. https://doi.org/10.1016/S0011-9164(00)00077-1.

[45] O.A. Akinbulumo, O.J. Odejobi, and E.L. Odekanle, "Thermodynamics and adsorption study of the corrosion inhibition of mild steel by *Euphorbia heterophylla* L. extract in 1.5 M HCl", *Results in Materials*, vol. 5, pp. 100074, 2020. https://doi.org/10.1016/j.rinma.2020.100074.

[46] I.B. Onyeachu, D.I. Njoku, S.C. Nwanonenyi, C.C. Ahanotu, and K.M. Etiowo, "Investigation into the adsorption and inhibition properties of sodium octanoate against CO_2 corrosion of C1018 carbon steel under static and hydrodynamic conditions", *Scientific African*, vol. 20, pp. e01603, 2023. https://doi.org/10.1016/j.sciaf.2023.e01603.

[47] S. Chaudhary, and R.K. Tak, "Natural corrosion inhibition and adsorption characteristics of Tribulus terrestris plant extract on aluminium in hydrochloric acid environment", *Biointerface Research in Applied Chemistry*, vol. 12, no. 2, pp. 2603–2617, 2022. https://doi.org/10.33263/BRIAC122.26032617.

[48] I.B. Onyeachu, M.A. Quraishi, I.B. Obot, and J. Haque, "Newly synthesized pyrimidine compound as CO_2 corrosion inhibitor for steel in highly aggressive simulated oilfield brine", *Journal of Adhesion Science & Technology*, vol. 33, pp. 1226-1247, 2019. https://doi.org/10.1080/01694243.2019.1585029.

[49] I. Milošev, "The effect of various halide ions on the passivity of Cu, Zn and Cu–xZn alloys in borate buffer", *Corrosion science*, vol. 49, no. 2, pp. 637-653, 2007. https://doi.org/10.1016/j.corsci.2006.06.009,

[50] A.C. Lazanas, and M.L. Prodromidis, "Electrochemical impedance spectroscopy: A tutorial", *ACS Measurement Science*, vol. 3, no. 3, pp. 162-193, 2023. https://doi.org/10.1021/acsmeasuresciau.2c00070.

[51] K.M. Ismail, A.M. Fathi, and W.A. Badawy, "Electrochemical behavior of copper–nickel alloys in acidic chloride solutions", *Corrosion Science*, vol. *48*, no. 8, pp. 1912-1925, 2006. https://doi.org/10.1016/j.corsci.2005.07.004.

[52] Y. Lu, H. Xu, J. Wang, and X. Kong, "Oxygen reduction mechanism on copper in a 0.5 M H_2SO_4", *Electrochimica Acta*, vol. 54, no. 15, pp. 3972-3978, 2009. https://doi.org/10.1016/j.electacta.2009.02.019.

[53] H. Gerengi, M. Mielniczek, G. Gece, and M.M. Solomon, "Experimental and quantum chemical evaluation of 8-hydroxyquinoline as a corrosion inhibitor for copper in 0.1 M HCl", *Industrial & Engineering Chemistry Research*, vol. 55, no. 36, pp. 9614-9624, 2016. https://doi.org/10.1021/acs.iecr.6b02414.

[54] K.M. Ismail, "Evaluation of cysteine as environmentally friendly corrosion inhibitor for copper in neutral and acidic chloride solutions", *Electrochimica Acta*, vol. 52, pp. 7811–7819, 2007. https://doi.org/10.1016/j.electacta.2007.02.053.

[55] B. Lu, J. Luo, and Y. Lu. "Correlation between film rupture ductility and PbSCC of Alloy 800", *Electrochim. Acta*, vol. 53, no. 12, pp. 4122–4136, 2008. https://doi.org/10.1016/j.electacta.2007.12.070

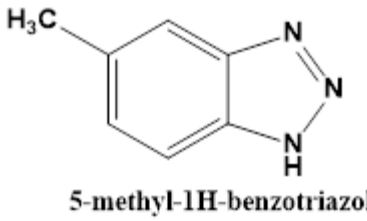

5-methyl-1H-benzotriazole

Figure 1. Molecular structure of corrosion inhibitor

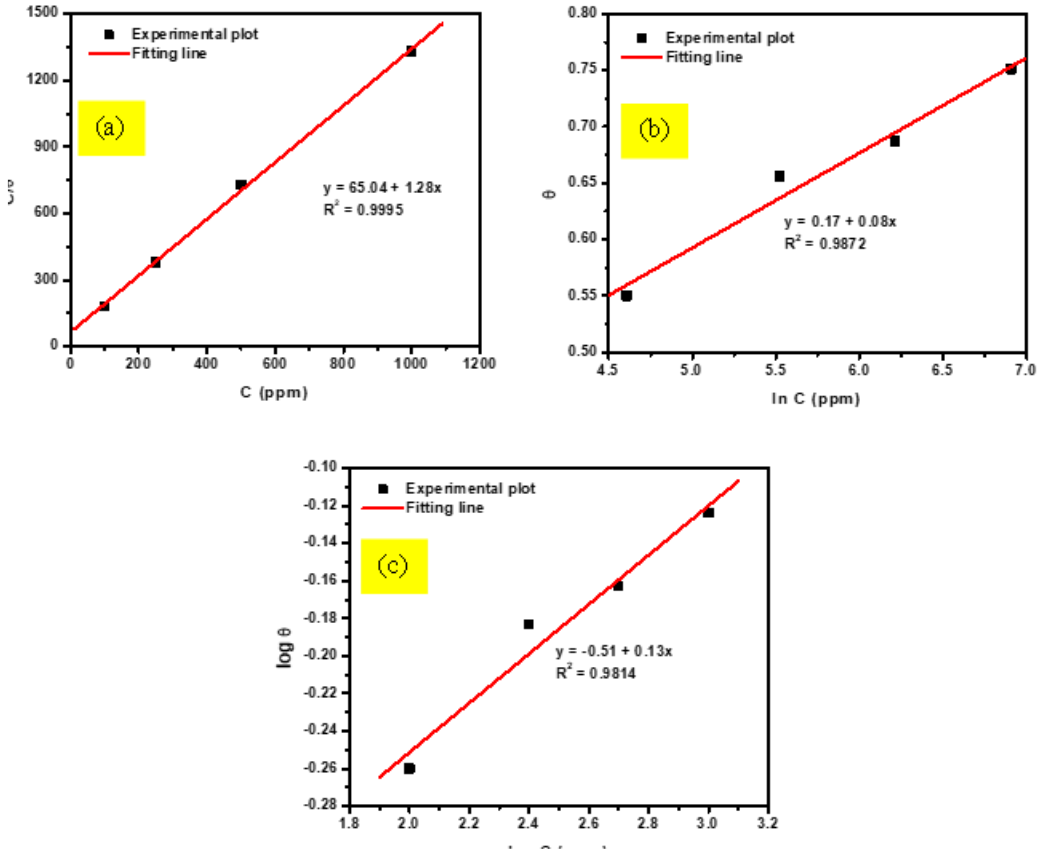

Figure 2. (a) Langmuir (b) Temkin and (c) Freundlich isotherm plots for the adsorption of MHB on 70-30 Cu-Ni alloy during corrosion in 1 M HCl.

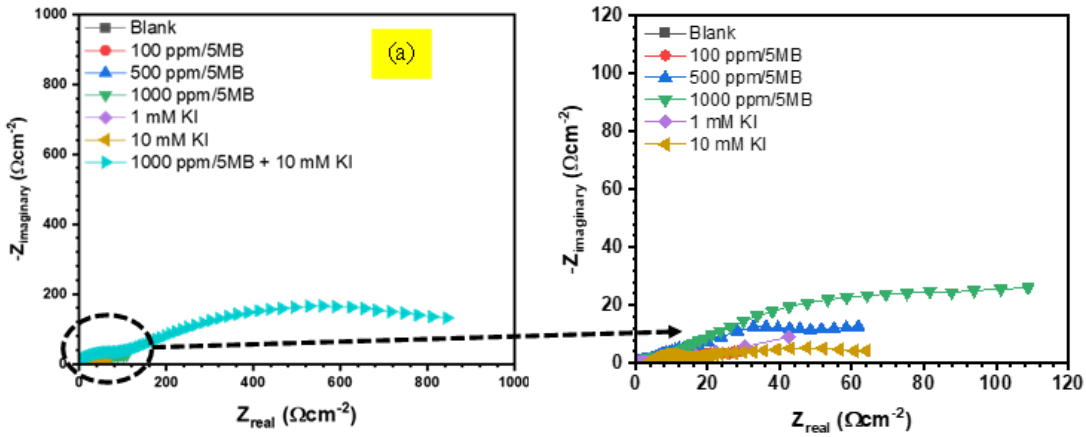

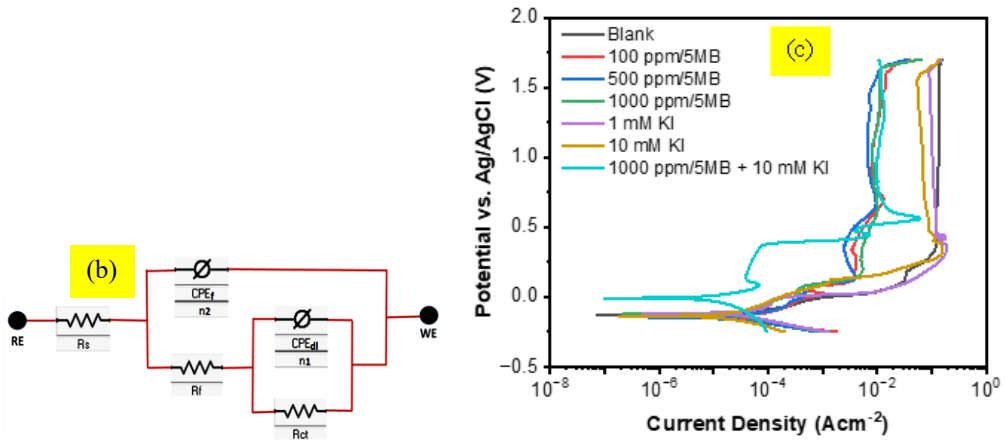

Figure 3. (a) EIS result presented in Nyquist format (b) Equivalent circuit model and (c) potentiodynamic polarization result after immersion of 70Cu-30Ni alloy in 1 M HCl.

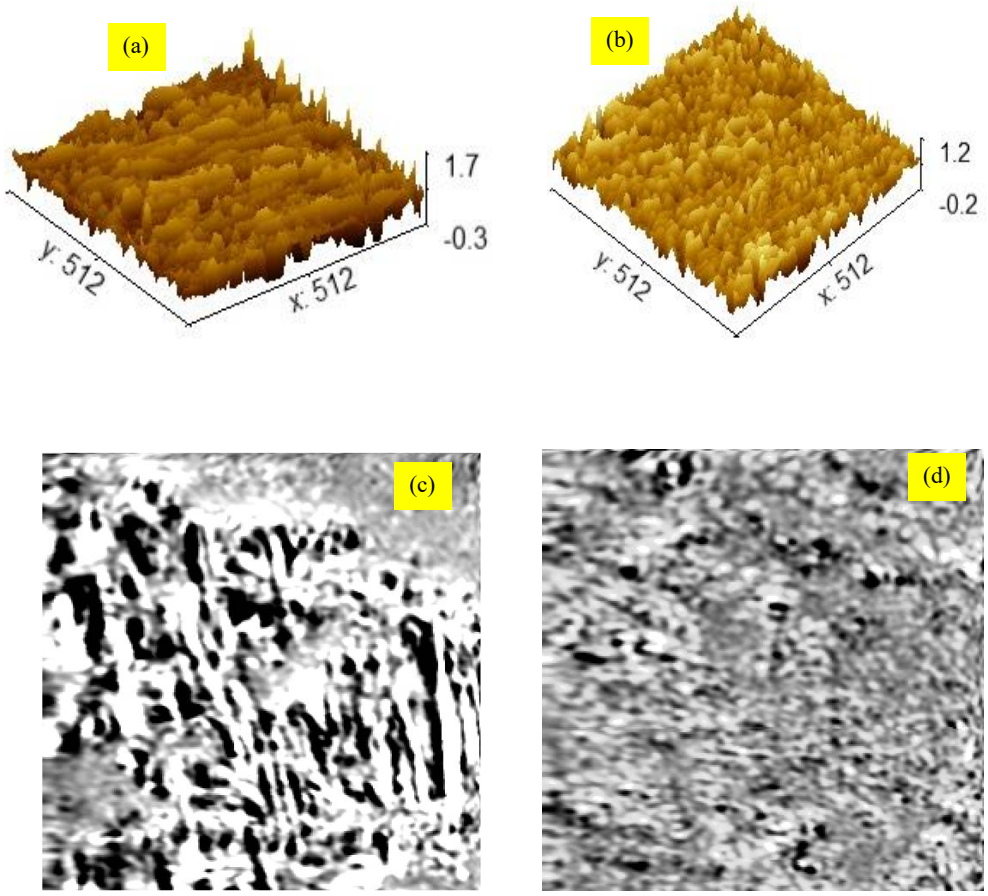

Figure 4. AFM and SEM images showcasing the surface profile of Cu-Ni alloy after 48 h immersion in 1 M HCl solution (a,c) without and (b,d) with 5MB + KI.

Table 1. Weight loss and corrosion rate experienced by 70Cu–30Ni after 48 h immersion in blank and inhibited acid.

Inhibitor	Conc. (5MB = ppm; KI = mM)	Weight loss (± S.D) (g)	Corrosion Rate (± S.D) (mm/yr)	IE (%)
	Blank	0.032 ± 0.007	0.289 ± 0.08	–
	100	0.030 ± 0.004	0.271 ± 0.05	6.25
5MB	250	0.011 ± 0.001	0.099 ± 0.02	65.63
	500	0.010 ± 0.004	0.090 ± 0.05	68.75
	1000	0.008 ± 0.001	0.072 ± 0.01	75.00
	1	0.020 ± 0.004	0.180 ± 0.05	37.50
KI	5	0.017 ± 0.004	0.153 ± 0.05	46.88
	10	0.013 ± 0.000	0.117 ± 0.00	59.38
5MB + KI	1000 + 10	0.002 ± 0.001	0.018 ± 0.01	93.75

Table 2. EIS parameters derived for the corrosion of 70Cu-30Ni in 1 M HCl without and with different inhibitor systems

Inhibitor	Conc. (5 MB = ppm; Ki - mM)	R_s (Ω cm^2)	CPE_{dl}		R_{ct} (Ω cm^2)	CPE_f		R_f (Ω cm^2)	($R_p = R_f + R_{ct}$) (Ω cm^2)	IE (%)
			Y_{dl} (mFcm^{-2} s^{n-1})	α_{dl}		Y_f (mFcm^{-2}sn^{-1})	α_f			
	Blank	0.90 ± 0.002	314 ± 0.05	0.76 ± 0.008	19.72± 2.96	0.95 ± 0.01	0.70 ± 0.001	7.56 ± 0.18	27.28	–
5MB	100	1,17 ± 0.001	5.24 ± 0.01	0.78 ± 0.000	20.24 ± 0.14	0.86 ± 0.00	0.80 ± 0.000	9.70 ± 0.000	29.94	8.88
	500	1.72 ± 0.014	3.20 ± 0.02	0.82 ± 0.002	67.90 ± 8.63	1.57 ± 0.00	0.80 ± 0.001	23.58 ± 4.85	91.48	70.18
	1000	1.91 ± 0.002	3.03 ± 0.06	0.82 ± 0.001	69.20 ± 6.54	0.67 ± 0.05	0.80 ± 0.000	34.72 ± 3.62	103.92	73.75
KI	10	1.20 ± 0.000	4.11 ± 0.26	0.76 ± 0.014	49.65 ± 1.42	1.52 ± 0.01	0.74 ± 0.011	18.64 ± 2.56	68.29	60.05
5MB + KI	1000 + 10	2.49 ± 0.013	0.01 ± 0.00	0.91 ± 0.000	552.90 ± 8.63	0.60 ± 0.01	0.90 ± 0.001	184.40 ± 6.36	737.30	96.30

Table 3. Polarization parameters derived for the corrosion of 70Cu-30Ni in 1 M HCl without and with different inhibitor systems.

Inhibitor	Conc. (5 MB = ppm; KI - mM)	E_{corr} (V/Ref)	i_{corr} (μA cm^{-2})	β_a (mV dec^{-1})	$-\beta_c$ (mV dec^{-1})	E_{pass} (V/Ref)	i_{pass} (mA cm^{-2})	% IE
	Blank	–0.122	38.60	54	80	+ 0.396	119.00	–
5 MB	100	–0.125	16.56	67	77	+ 0.351	3.50	58.00
	500	–0.127	12.89	65	78	+ 0.350	2.53	66.61
	1000	–0.122	10.50	73	88	+ 0.357	2.79	72.80
KI	1 mM KI	–0.129	25.01	64	87	+ 0.511	112.00	35.21
	10 mM KI	–0.117	17.37	69	83	+ 0.410	22.60	55.00
5MB + KI	1000 ppm + 10 mM KI	–0.003	3.07	91	72	+ 0.348	2.11	92.05